Chaos, Solitons and Fractals 174 (2023) 113761

Contents lists available at ScienceDirect

Chaos, Solitons and Fractals

journal homepage: www.elsevier.com/locate/chaos

Tricritical behavior in epidemic dynamics with vaccination

Marcelo A. Pires [a,*], Cesar I.N. Sampaio Filho [b], Hans J. Herrmann [b,c], José S. Andrade Jr. [b]

[a] Universidade Federal de Alagoas, Campus do Sertão, 57480-000, Delmiro Gouveia AL, Brazil
[b] Universidade Federal do Ceará, Campus do Pici, 60451-970, Fortaleza CE, Brazil
[c] PMMH, ESPCI, 7 quai St. Bernard, 75005 Paris, France

ARTICLE INFO

Keywords:
Critical
Tricritical
Vaccination
Epidemics

ABSTRACT

We scrutinize the phenomenology arising from a minimal vaccination-epidemic (MVE) dynamics using three methods: mean-field approach, Monte Carlo simulations, and finite-size scaling analysis. The mean-field formulation reveals that the MVE model exhibits either a continuous or a discontinuous active-to-absorbing phase transition, accompanied by bistability and a tricritical point. However, on square lattices, we detect no signs of bistability, and we disclose that the active-to-absorbing state transition has a scaling invariance and critical exponents compatible with the continuous transition of the directed percolation universality class. Additionally, our findings indicate that the tricritical and crossover behaviors of the MVE dynamics belong to the universality class of mean-field tricritical directed percolation.

1. Introduction

The current pandemic revealed that disease spreading still poses several challenges for society. In order to combat an epidemic spreading, vaccination is a great ally [1]. As many social and biological processes, epidemic and vaccination dynamics can be addressed with tools from statistical physics due to the stochastic nature of the disease spreading [2–5].

From the statistical physics point of view, epidemic processes undergo nonequilibrium phase transitions [6,7]. Nonequilibrium physics is not a simple extension of equilibrium physics, but is associated with new phenomena. There exist many epidemic models [1,2] and the SIS (Susceptible–Infected–Susceptible) is the paradigmatic model that presents a phase transition from an active phase, where there is a self-sustaining perpetuation of the disease in the population, to an absorbing phase, where the disease is eradicated. The nonequilibrium phase transition of the SIS model is continuous (second-order) and follows the behavior of the important directed percolation (DP) universality class of absorbing-state transitions [7]. The DP universality class includes not only epidemic processes, but a large variety of spreading phenomena observed in Nature [6].

As aforementioned, vaccination is a key tool to mitigate the impact of a disease spreading. In mathematical modeling, vaccination can be minimally coupled to the SIS models by introducing the vaccinated compartment, V, with the corresponding rates. In such case, vaccination induces an increase in the epidemic threshold, reducing the impact of a self-sustaining chain of contagion. This effect preserves the continuous nature of the SIS phase transition as shown, for instance, in [8–11]. Nevertheless, due to the fact that all vaccines have a limited effectiveness, the nature of this transition can change if a vaccinated individual becomes infected, passing directly from compartment V to I [12]. Following this work, subsequent models for epidemics with vaccination exhibiting both continuous and discontinuous transitions have been extensively studied in the mathematical community by means of the forward–backward bifurcation theory [13–25]. However, the overwhelming majority of such studies have focused on deterministic models considering fully-mixed populations. Here, we investigate the statistical and spatial properties of a minimal vaccination-epidemic model by means of three methods: Monte Carlo simulations, finite-size scaling (FSS) and mean-field approach. As we will see, our findings revealed the presence of continuous and discontinuous phase transitions depending on the system's dimensionality.

This work is organized as follows. In Section 2, we describe our stochastic minimal vaccination-epidemic (MVE) model with the corresponding mean-field treatment. In Section 3, we present the results and discussion from Monte Carlo (MC) simulations and scaling theory. Final remarks are presented in Section 4.

2. Model

Minimal models can be highly instructive in providing insights that can help to elucidate the mechanisms inherent in the large-scale behavior of a given system [26]. In this sense, we consider a statistical

* Corresponding author.
E-mail address: marcelo.pires@delmiro.ufal.br (M.A. Pires).

https://doi.org/10.1016/j.chaos.2023.113761
Received 26 March 2023; Received in revised form 18 June 2023; Accepted 25 June 2023
Available online 12 July 2023

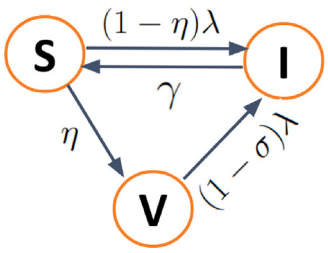

Fig. 1. Sketch of the vaccination dynamics with an illustration of the probabilities $\{\lambda, \eta, \gamma, \sigma\}$ described in the text. For brevity, we call this model as minimal vaccination-epidemic (MVE) dynamics. The MVE model is composed by four compartmental transitions: (i) two activated by a pairwise interaction ($S + I \to 2I$ and $V + I \to 2I$); and (ii) two non-mediated by interactions ($S \to V$ and $I \to S$).

and minimal version of the model presented in Ref. [17]. Our model is sketched in Fig. 1. The N individuals of a population can be divided into 3 states: Susceptible (S), Infected (I) and vaccinated (V). If a given individual i is susceptible, a vaccination event $S \to V$ takes place with probability η. If i does not get vaccinated (event that takes place with probability $1-\eta$) then i becomes infected with probability λ_{ef}. For a full graph $\lambda_{ef} = \lambda I/N$, whereas for structured graphs we need to consider the number of infected neighbors, $n_I(i)$. For the square lattices $\lambda_{ef} = \lambda n_I(i)/4$ and for the random k-regular graphs $\lambda_{ef} = \lambda n_I(i)/k$. If an individual i is already vaccinated and meets an infected peer, then a contagion event takes place with probability $(1-\sigma)\lambda_{ef}$, where σ is the vaccine effectiveness. If $\sigma = 1$ the vaccine has 100% of effectiveness. In turn, the infected individuals recover becoming susceptible again, $I \to S$, with probability γ. We assume that the virus mutates fast having many variants so that an infection is not sufficient to effectively induce immunity. For this reason, we ignore any transition from compartment I to V.

2.1. Mean-field approach

From the previously stated concepts and rules, as illustrated in Fig. 1, we obtain the mean-field equations:

$$\frac{dS}{dt} = -\eta S - (1-\eta)\lambda S\frac{I}{N} + \gamma I \tag{1}$$

$$\frac{dI}{dt} = (1-\eta)\lambda S\frac{I}{N} + (1-\sigma)\lambda V\frac{I}{N} - \gamma I \tag{2}$$

$$\frac{dV}{dt} = \eta S - (1-\sigma)\lambda V\frac{I}{N}, \tag{3}$$

where we denote by S, I and V the number of individuals in the compartments $\{S, I, V\}$, respectively. Adding the Eqs. (1)–(3) we obtain $\frac{dS}{dt} + \frac{dI}{dt} + \frac{dV}{dt} = 0$ as expected since $N = S + I + V$ is assumed constant.

The Eqs. (1)–(3) accompanied by $N = S + I + V$ provide a steady-state governed by a third-degree polynomial

$$\rho_\infty\left(A\rho_\infty^2 + B\rho_\infty - C\right) = 0, \tag{4}$$

where $\rho_\infty = I_\infty/N$ and

$$A = (1-\sigma)\lambda(1-\eta) \tag{5}$$

$$B = (1-\sigma)(\gamma + \eta - \lambda(1-\eta)) \tag{6}$$

$$C = \eta\left(1 - \sigma - \frac{\gamma}{\lambda}\right). \tag{7}$$

The 3 solutions of Eq. (4) are:

$$\rho_\infty^o = 0 \tag{8}$$

$$\rho_\infty^\pm = \frac{-B}{2A} \pm \sqrt{\frac{C}{A} + \left(\frac{B}{2A}\right)^2}. \tag{9}$$

The above equations are very instructive.

First, the Eq. (5) shows that $A \geq 0$ for any choice of the epidemic parameters that are bounded between 0 and 1. This observation simplifies the stability analysis. The solution $\rho_\infty^o = 0$ corresponds to an absorbing state, the disease-free phase. From a linear stability analysis one finds that ρ_∞^o is stable for $C > 0$ and unstable for $C < 0$. At $C = 0$ we obtain the critical point $\lambda_c = \frac{\gamma}{1-\sigma}$. The system undergoes a continuous active-absorbing-state phase transition at $\lambda = \lambda_c$, if $B > 0$ where the solution ρ_∞^+ becomes stable. In this case, close to the critical point (critical region) we find that the order parameter behaves as $\rho_\infty \sim \left(\lambda - \lambda_c\right)^{\beta_{DP}}$, with $\beta_{DP} = 1$. If $B < 0$ the transition becomes discontinuous and there is a region $\lambda_c \leq \lambda \leq \lambda^*$ characterized by a bistability between the solutions ρ_∞^o and ρ_∞^+. At $B = 0$ we find the tricritical point (TCP) $\lambda_T = \frac{\gamma+\eta}{1-\eta}$. At the TCP $\lambda_T = \lambda_c$ thus $\sigma_T = 1 - \frac{\gamma(1-\eta)}{\gamma+\eta}$. As a consequence, close to the TCP (tricritical region) we find that the order parameter behaves as $\rho_\infty \sim \left(\lambda - \lambda_T\right)^{\beta_T}$ with $\beta_T = 1/2$. Finally, the solution ρ_∞^- yields unphysical and unstable results. For further reference, we summarize the location of the TCP,

$$(\lambda_T, \sigma_T) = \left(\frac{\gamma+\eta}{1-\eta}, \frac{\gamma+\eta+\gamma(1-\eta)}{\gamma+\eta}\right). \tag{10}$$

Second, if $A = 0$ the higher-order term in Eq. (4) disappears which in turn removes any possibility for a discontinuity in the epidemic transition for this model. From Eq. (5) we see that $A = 0$ if the vaccination program is operated with a 100% effective vaccine, *i.e.* $\sigma = 1$. In any case, even if $\sigma < 1$ the abrupt transition to the spreading phase can be suppressed if the vaccination probability is sufficiently high, $\eta \geq \eta^\dagger$. By setting $\lambda_T = \frac{\gamma+\eta^\dagger}{1-\eta^\dagger} = 1$ we obtain explicitly the threshold

$$\eta^\dagger = \frac{1-\gamma}{2} \tag{11}$$

2.2. Simulation on complete graphs

We employ the Gillespie's algorithm [27] to obtain the time evolution of the model on complete graphs. In this algorithm the time to the next event is exponentially distributed and the probability of each event is proportional to its rate. We define N_S, N_I and N_V as the number of Susceptible, Infected and Vaccinated individuals, respectively. At each time t we compute the rate of each event described in the previous subsection: $r_1 = r_{S\to V} = \eta N_S$, $r_2 = r_{S\to I} = (1-\eta)\lambda N_S N_I/N$, $r_3 = r_{V\to I} = (1-\sigma)\lambda N_V N_I/N$, $r_4 = r_{I\to S} = \gamma N_I$. Next, we compute the sum of all process rates $r_{tot} = \sum_{i=1}^{i=4} r_i$. We determine the time increment δt by generating a random number from an exponential distribution with parameter r_{tot}, *i.e.*, $\delta t \sim \exp(r_{tot})$. The next event i is chosen with probability directly proportional to its rate, *i.e.*, we sample the next event i uniformly with probability $p_i = r_i/r_{tot}$. Such probability distribution ensures that $\sum_{i=1}^{i=4} p_i = 1$. Subsequently, the population variables are updated according to the type of event to be selected:

- (E1) If the event $S \to V$ is chosen, N_S is decreased by one and N_V is increased by one;
- (E2) If the event $S \to I$ is selected, one unit is subtracted from N_S and one unit is added to N_I;
- (E3) If the event $V \to I$ is sampled, N_V is decreased by one and N_I is increased by one;
- (E4) If the event $I \to S$ is picked, one unit is subtracted from N_I and one unit is added to N_S.

These steps are performed while $t \leq t_{max}$.

2.3. Simulation on structured graphs

During the simulation of the MVE model on square lattices and random k-regular graphs we use two lists: (a) $\mathcal{L}_I$: list of infected individuals with size N_I; (b) $\mathcal{L}_S$: list of susceptible individuals with size N_S. Denote δt as a time increment associated with a given step in the simulation. At each step one of the following events can take place:

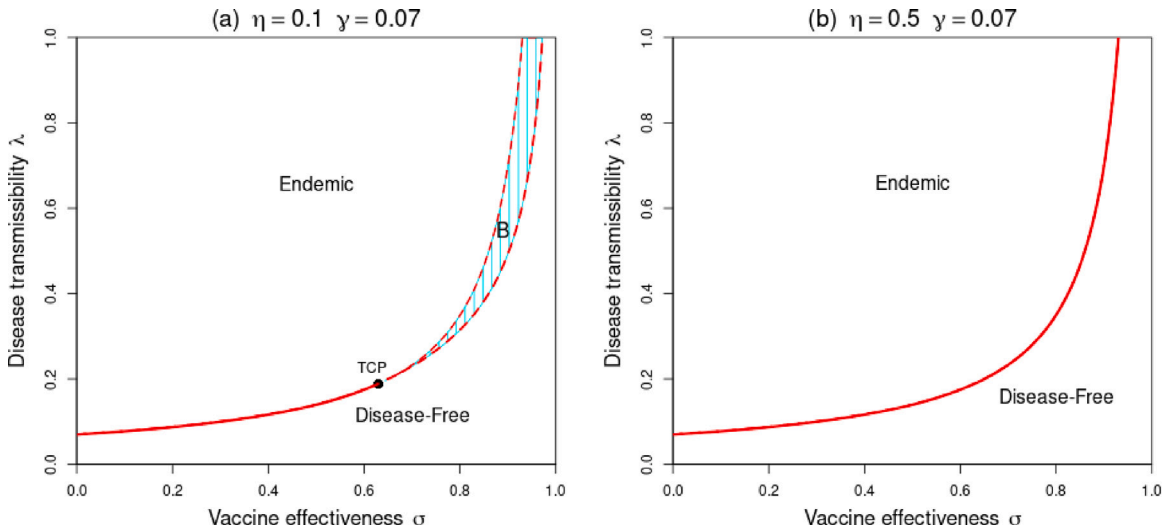

Fig. 2. Mean-field phase diagram of the minimal vaccination-epidemic (MVE) model, as depicted in Fig. 1, for $\gamma = 0.07$, and: $\eta = 0.1$ (a) and $\eta = 0.5$ (b). The shaded area corresponds to the bistable (B) phase where the dynamics has three fixed points: two stable (ρ_∞^+ and ρ_∞^o) and one unstable (ρ_∞^-). In the Disease-Free phase ρ_∞^o is the only the stable fixed point. In turn, ρ_∞^+ is the unique stable fixed point in the Endemic phase. The coordinates of the tricritical point (TCP) are obtained from Eq. (10). From the thresholds of $\rho_\infty^\pm$ in Eq. (9), we obtain the solid and dashed curves that represent continuous and discontinuous transitions, respectively. The bistability can be suppressed if the vaccination probability η is above the threshold given by the Eq. (11).

(E1) Vaccination of a susceptible individual with probability $\eta N_S \delta t$. In this case, we choose randomly an individual i from $\mathcal{L}_S$. The state of i changes as $S \to V$.

(E2) Infection of a susceptible individual with probability $(1-\eta)\lambda N_I \delta t$. For this event, we pick at random an individual i from $\mathcal{L}_I$. Then, we choose randomly a neighbor j of i. If j is susceptible, the state of such individual changes as $S \to I$.

(E3) Infection of a vaccinated individual with probability $(1-\sigma)\lambda N_I \delta t$. In this event, we sample uniformly an individual i from $\mathcal{L}_I$. Then, we select at random a neighbor j of i. If j is vaccinated, the state of such individual changes as $V \to I$.

(E4) Recovery of an infected individual with probability $\gamma N_I \delta t$. In this case, we sample uniformly an individual i from $\mathcal{L}_I$. The state of i changes as $I \to S$.

Then, we increase the time t by an amount δt. From the normalization of the total probability we obtain $\frac{1}{\delta t} = \eta N_S + (2 - \eta - \sigma)\lambda N_I + \gamma N_I$. These steps are performed while $t \leq t_{max}$.

2.4. Further simulation details

In epidemic models, the absorbing state refers to the configuration without infected individuals. If this state is reached, the dynamics stops. However, in finite systems the absorbing configuration can always be achieved, even in the supercritical phase. To avoid this issue, we apply a quasi-stationary method to characterize the dynamics of the model. Specifically, we apply a reactivation method [28,29] in which we perform a reinfection of one individual (randomly chosen) every time the dynamics reaches the absorbing configuration.

In our simulations we consider a complete graph (also called full graph or fully-connected network) that is a structure where each vertex (individual) interacts with all others. We also consider a random k-regular graph that is a quenched structure where each node has k neighbors. Finally, we consider a square lattice of lateral size L with a von Neumann neighborhood (4 neighbors) and periodic boundary conditions.

For the finite-size scaling (FSS) analysis of the MVE model we start all simulations with the system fully occupied with infected individuals and we follow the procedures delineated above (see also Section 3.4.3 of Ref. [7]).

By means of stochastic simulations, we compute the fraction of infected agents which is the order parameter ρ of the model

$$\rho = \left\langle \frac{1}{N} \sum_{i=1}^{N} x_i \right\rangle, \tag{12}$$

where $x_i = 1$ if i is infected, otherwise $x_i = 0$ and $\langle \dots \rangle$ denotes the average over $n_{samples} = 10^2$ samples for each parameter setting.

3. Results and discussion

In this section, we first provide an analysis of the parameter space for the mean-field setup. Next, we focus on the parameter configurations that produce a large discontinuity in mean-field results. That is, we set $\gamma = 0.07$, $\eta = 0.1$ and $\sigma = 0.9$ in all the finite-size simulations, when not stated otherwise.

In Fig. 2, we show two typical phase diagrams of the MVE model illustrated in Fig. 1. In the panel (a) with $\eta = 0.1$, we observe in the phase diagram that the transition from the disease-free phase to the spreading one is continuous if $\sigma \leq \sigma_T$ or discontinuous if $\sigma > \sigma_T$. Such discontinuity in the order parameter, infected density, is not found in the phase diagram of panel (b) because in this case the vaccination probability $\eta = 0.5$ is greater than the threshold value given by Eq. (11), $\eta^\dagger = (1-\gamma)/2 = 0.465$. That is, prevention of an abrupt spread of an epidemic can be achieved if the vaccination probability is high enough.

In Fig. 3, we show the long-time behavior of the order parameter ρ versus the control parameter λ considering three structures: complete graphs, random k-regular networks and square lattices. The simulations in the upper branch started with $\lambda = 0.7$ and $\rho_o = 1$, while the simulations in the lower branch started with $\lambda = 0.49$ and $\rho_o = 1/N$. We then increase (or decrease) λ by a constant amount $\Delta\lambda = 0.01$ with a new initial condition corresponding to the final configuration of the preceding simulation. The results for complete graphs [Fig. 3(a)] and random k-regular networks [Fig. 3(b)] reveal the presence of a hysteresis loop, history-dependence of the dynamics, which is a signature of a first-order transition. These results are in agreement with the corresponding mean-field prediction, as expected, since complete graphs and random k-regular networks are infinite-dimensional systems. On the other hand, for the simulations on the square lattice [Fig. 3(c)], we did not find differences between the upper and lower branches, which in turn suggests the absence of hysteresis and of a discontinuous transitions

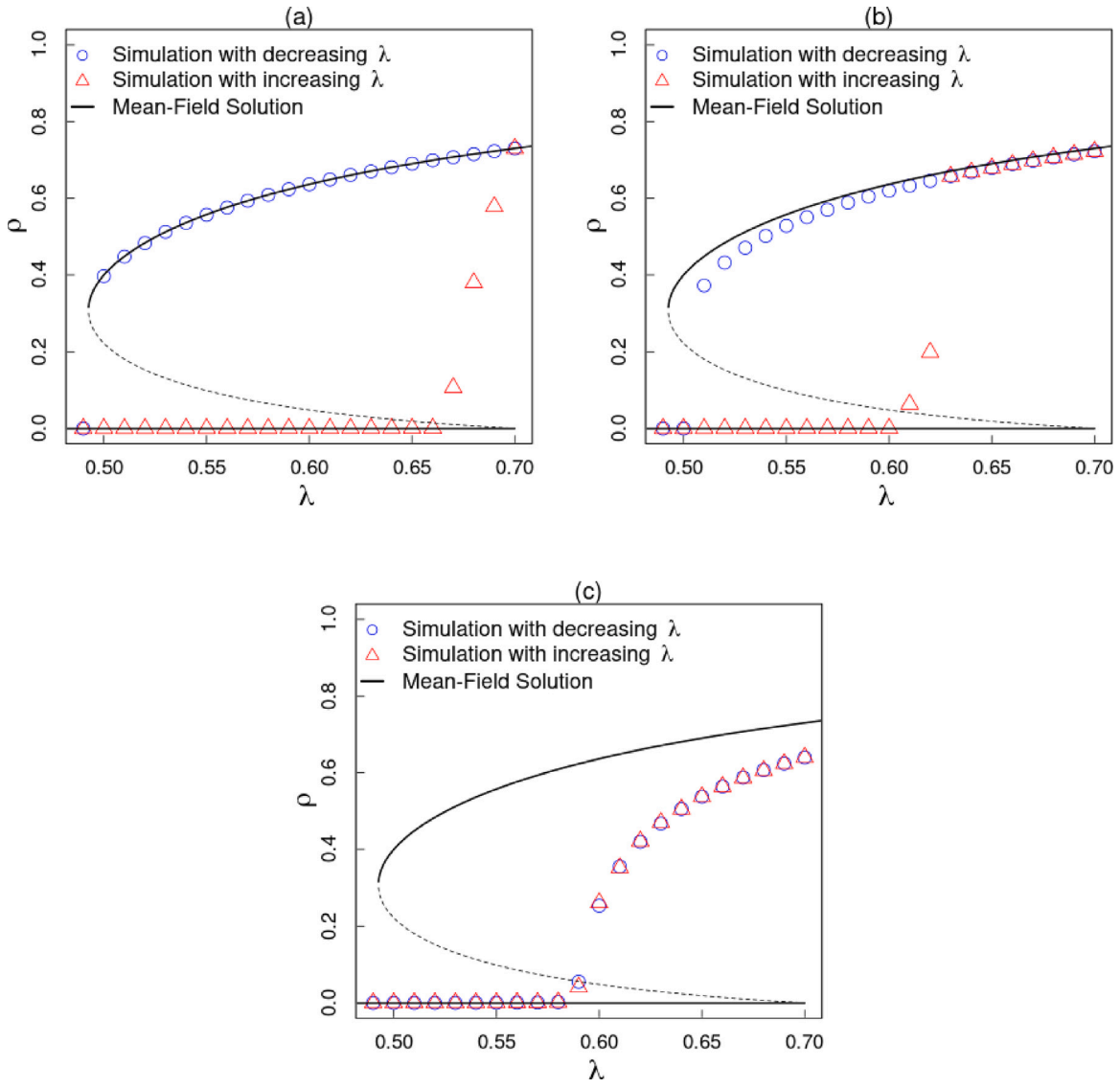

Fig. 3. Stationary infected density ρ versus the transmissibility λ for the MVE model on: (a) complete graphs, (b) random k-regular networks with $k = 20$, (c) square lattice. Simulations performed with $t_{max} = 10^5$ on structures with $N = 10^4$ individuals each. The control parameter λ is increased (red triangles) and decreased (blue circles) in the range $0.49 \leq \lambda \leq 0.7$ at constant intervals of $\Delta\lambda = 0.01$. In the upper branch the simulations started with $\lambda = 0.7$ from $\rho_o = 1$ (fully active initial condition), whereas in the lower branch the simulations started with $\lambda = 0.49$ from $\rho_o = 1/N$ (localized initial condition). The stable and unstable theoretical solutions, obtained from the Eq. (9), are represented in the solid and dashed lines, respectively.

for the MVE model on this two-dimensional lattice. Moreover, these findings underscore the dependence of hysteresis on the dimensionality of the system.

The sensitivity of the stationary order parameter to initial conditions is another test that provides clues about the nature of absorbing-state phase transitions for a given set of parameters [29,30]. The results of such a test are shown in Fig. 4 where we plot several time series of the infected density ρ for initial conditions in the interval $[1/N, 1]$. The simulations on full graphs [Fig. 4(a)] and random k-regular networks [Figs. 4(b)] reveal that the stationary state depends on the initial conditions in a bistable mode. Such bistability confirms that the MVE model undergoes a discontinuous phase transitions on structures with infinite dimension. On the other hand, on square lattices [Fig. 4(c)] all the time series of ρ converge to a single stationary state for all the considered initial conditions ρ_o. These results indicate that the spatial constraints in 2D lattices possess the capacity to disrupt the bistability of a dynamic process. Such absence of bistability provides further evidence that the phase transition of the MVE model remains continuous in this two-dimensional structure.

In Fig. 5 we provide a finite-size scaling (FSS) analysis of the MVE model on square lattices. From now on, we set $\rho_o = 1$ in all simulations. In Fig. 5(a) we plot $\ln \rho(t)$ versus $\ln t$ for different values of λ to monitor the deviations from the asymptotic power-law decay $\rho(t) \sim t^{-\delta}$ where δ is the critical density decay exponent. The positive (negative) curvature for large t indicates that the system has a tendency to reach the active (absorbing) phase. From the fit with the smallest curvature we find that the critical behavior in time $\rho(t) \sim t^{-\delta}$ holds satisfactorily with $\delta = 0.489 \pm 0.082$ and $\lambda_c = 0.5898 \pm 0.0005$ for a sufficiently large value of t.

Still in Fig. 5 we employ the data collapse technique for estimating other critical exponents. The scaling hypothesis predicts that all properly scaled curves can be collapsed onto a single curve. To perform a data collapse we invoke the following scaling laws [7],

$$\rho(t) \sim t^{-\beta/\nu_\parallel} \mathcal{F}(\Delta t^{1/\nu_\parallel}) \tag{13}$$

$$\rho(t) \sim L^{-\beta/\nu_\perp} \mathcal{G}(t L^{-z}), \tag{14}$$

where $\Delta = \lambda - \lambda_c$ is the deviation from the critical point, and $\mathcal{F}$ and $\mathcal{G}$ are scaling functions. In turn, z is the so-called dynamic critical

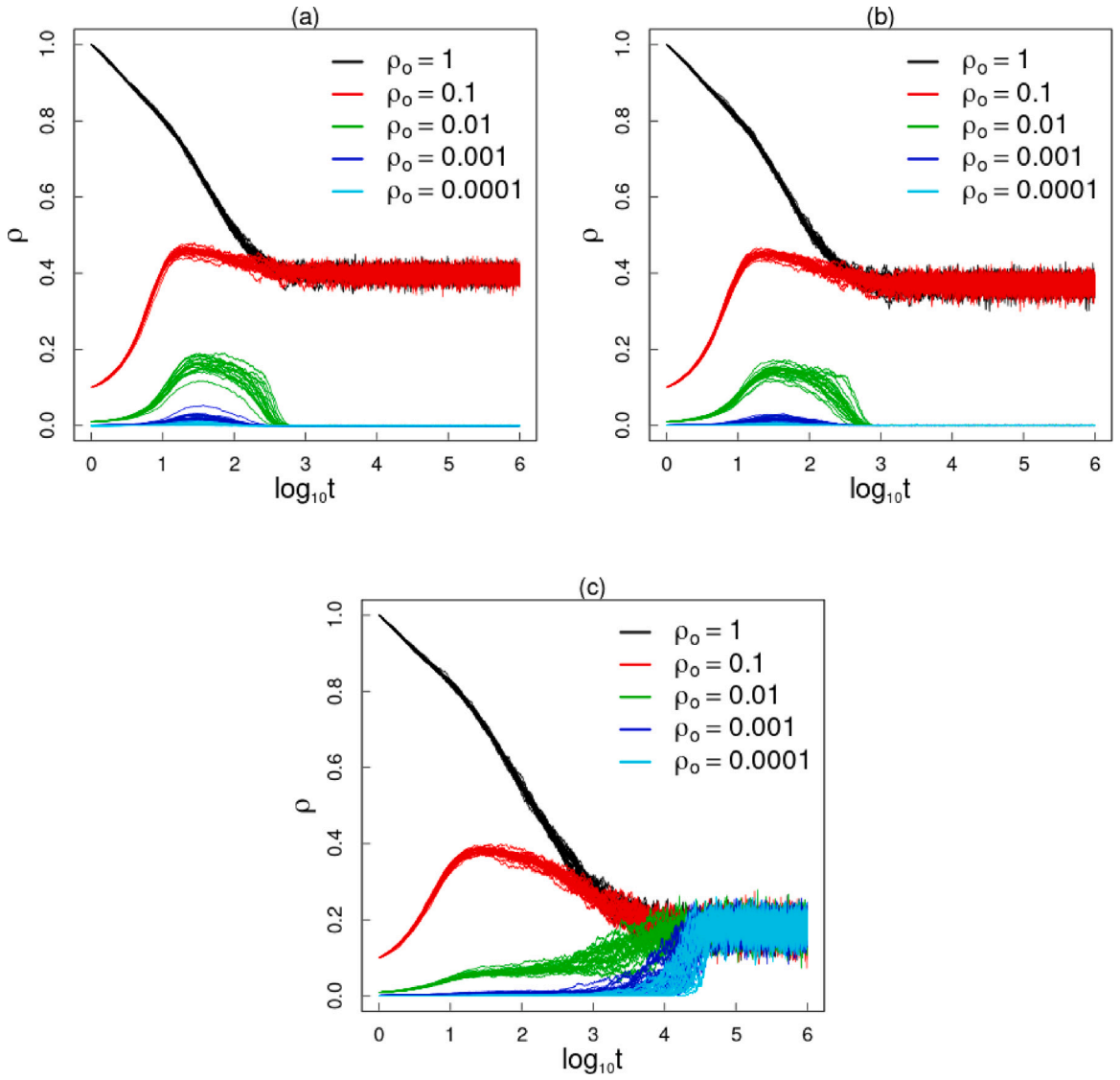

Fig. 4. Time evolution of the order parameter ρ for several initial conditions ρ_o. (a) $\lambda = 0.50$, complete graphs, (b) $\lambda = 0.51$, random k-regular networks with $k = 20$, (c) $\lambda = 0.595$, square lattice. All structures with $N = 10^4$ individuals. Each panel has 100 samples, and for better detecting eventual bistability we plot the time series for each parameter setting without averages. The time series in panels (a–b) exhibit bistable solutions, whereas the panel (c) exhibits a single stable steady state. In panels (a–b) note that in some dynamic scenarios, the presence of pronounced epidemic peaks in the short-term does not necessarily promote persistence of the transmission chain in the long-term.

exponent, whereas $\nu_\parallel$ and $\nu_\perp$ are the critical exponents associated with the temporal and spatial correlation lengths, respectively. Based on Eq. (13) we plot $\ln(\rho(t)t^{\beta/\nu_\parallel})$ versus $\ln(t\Delta^{\nu_\parallel})$ for different values of Δ as depicted in Fig. 5(b). Scanning several candidates for $\{\beta, \nu_\parallel\}$ we find that all curves collapse on a single curve for $\beta = 0.58 \pm 0.02$ and $\nu_\parallel = 1.29 \pm 0.01$. Based on Eq. (14), the scaled order parameter $\rho(t)L^{\beta/\nu_\perp}$ is plotted against tL^{-z} for various system sizes in the double-logarithmic graph shown in Fig. 5(c). By tuning $\{z, \beta, \nu_\perp\}$ the data points collapse onto a single curve for a sufficiently large value of t, which gives the estimated values $z = 1.73 \pm 0.12$, $\beta = 0.58 \pm 0.05$ and $\nu_\perp = 0.74 \pm 0.04$.

Taking a big-picture look at the results shown in the panels of Fig. 5, we note that the independent estimates for critical exponents are statistically consistent with each other. The best estimated values are summarized in Table 1. In many nonequilibrium models the triplet $\{\beta, \nu_\parallel, \nu_\perp\}$ is the fundamental set of critical exponents that labels the universality class [7]. The other critical exponents can be obtained from the relations $z = \nu_\parallel/\nu_\perp$ and $\delta = \beta/\nu_\parallel$. From Table 1 it is clear that our estimated critical exponents do satisfy these relations within the error bars. It is evident that the active-to-absorbing state transition of the MVE model on square lattices exhibits a scaling invariance with critical exponents compatible with the continuous transition of the directed percolation universality class. Moreover, the results of the 2D-MVE dynamics provides another support to the DP conjecture of Janssen [31] and Grassberger [32], which states that under very general circumstances [7] (scalar order parameter, short-range interactions and no special attributes such as additional symmetries or quenched randomness) models that exhibit a continuous phase transition from a fluctuating active phase into a *single* absorbing state should belong to the DP universality class.

The tricritical point (TCP) is the location in the phase diagram that separates continuous from discontinuous transitions. At the TCP a new universality class emerges [33–36]. In our case, sufficiently away from the TCP we observe that the MVE model belongs to the DP universality class. Then at the TCP we should expect a universal behavior according to the Tricritical Directed Percolation (TDP) universality class [37,38]. Indeed, this is what we observe in the results compiled in the panels of Fig. 6 and Table 2.

In Fig. 6 we provide the tricritical analysis of the MVE on full graphs. As we did not detect discontinuous transitions in the MVE model on square lattices, the tricritical analysis does not apply to

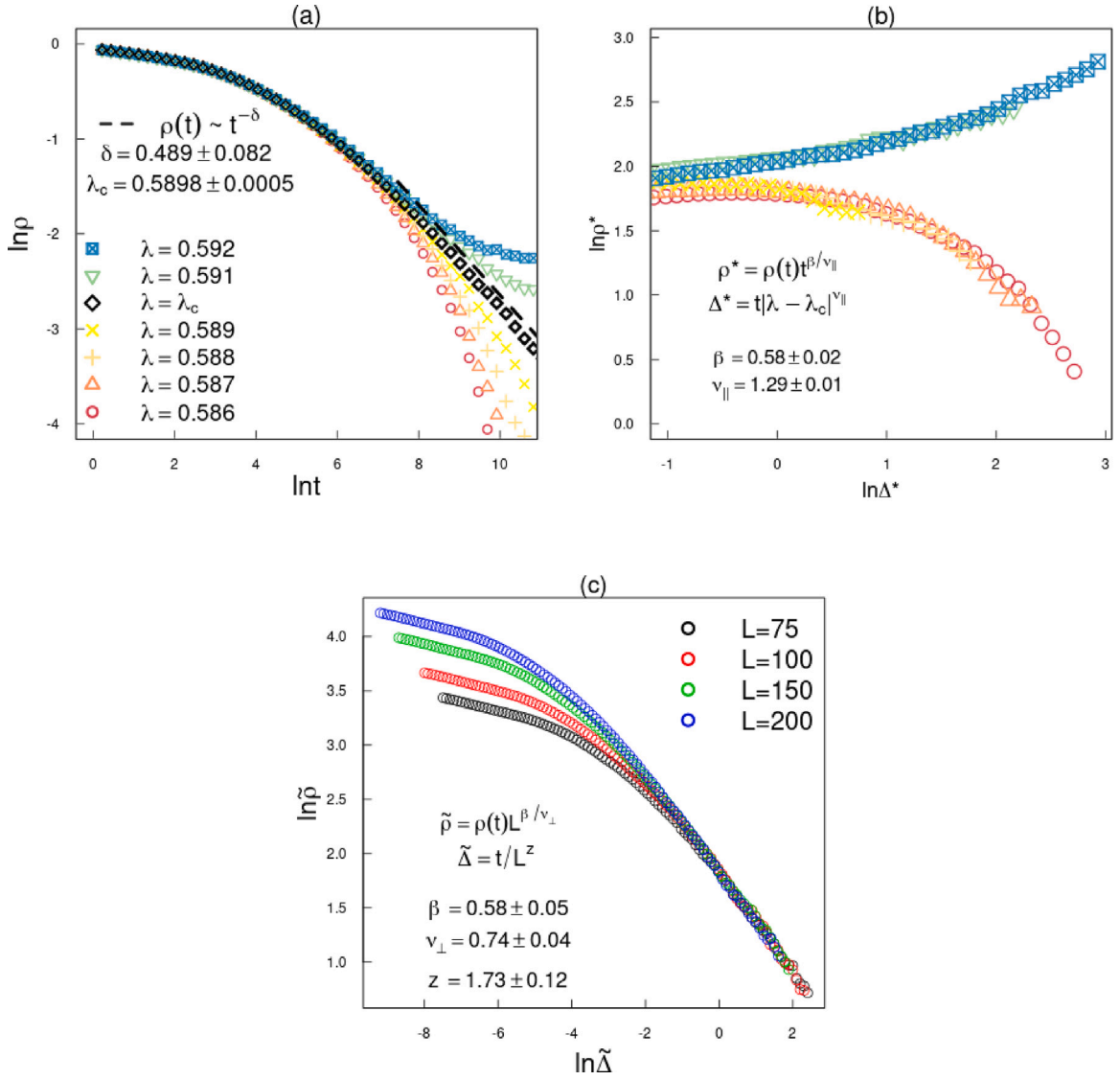

Fig. 5. Critical behavior of the MVE on square lattices. All panels are in log–log scale. Panel (a): $\rho(t)$ versus t for simulations performed with $L = 100$ and several λ around the critical point; the black dashed line corresponds to the fit with the least curvature. Panel (b): $\rho^* = \rho(t)t^{\beta/\nu_\parallel}$ versus $\Delta^* = t(\lambda - \lambda_c)^{\nu_\parallel}$ for simulations with $L = 100$; the color legend of panel (a) also applies to panel (b). Panel (c): $\tilde{\rho} = \rho(t)L^{\beta/\nu_\perp}$ versus $\tilde{\Delta} = tL^{-z}$ for simulations performed with $L = \{75, 100, 150, 200\}$. In panels (b–c) we use the λ_c estimated with the procedure shown in panel (a). In all cases we use $\rho_o = 1$ and we let the simulations run until the dynamics reaches the stationary state. The estimated critical quantities are shown inside each panel and the best estimates are compiled in the Table 1. (For interpretation of the references to color in this figure legend, the reader is referred to the web version of this article.)

these systems. Again, we start all MC simulations from $\rho_o = 1$. To assist our FSS analysis, we use some exact results from the mean-field calculations, namely the location of the TCP given by Eq. (10) with $\eta = 0.1$ and $\gamma = 0.07$: $(\lambda_T, \sigma_T) = (0.18889, 0.62941)$. In the panel (a) we show that the power-law decay $\rho(t) \sim t^{-\delta^T}$ is statistically satisfied at λ_T for the estimated exponent $\delta^T = 0.509 \pm 0.013$. Afterward, we employ a data collapse method for estimating other tricritical exponents. In Fig. 6(b) we plot $\rho(t)t^{-\beta^T/\nu_\parallel^T}$ versus $t\Delta^{\nu_\parallel^T}$ for several distances from the TCP, $\Delta = \lambda - \lambda_T$. We find that all curves collapse for the set $\beta^T = 0.50 \pm 0.01$ and $\nu_\parallel^T = 1.01 \pm 0.02$. In Fig. 6(c) the rescaled order parameter $\rho(t)N^{\beta^T/\nu_\perp^T}$ is plotted against t/N^{z^T} for various system sizes. By tuning $\{z^T, \beta^T, \nu_\perp^T\}$ the data points collapse onto a single curve for a sufficiently large value of t, which gives the estimated values $z^T = 1.9 \pm 0.2$, $\beta^T = 0.50 \pm 0.02$ and $\nu_\perp^T = 0.49 \pm 0.03$.

Let us now focus on the panel (d) of Fig. 6 where we perform the crossover analysis [37] based on the crossover scaling ansatz for the order parameter given by

$$\rho \sim \Delta_\sigma^{\beta^T/\phi^T} \mathcal{H}(\Delta_\lambda \Delta_\sigma^{-1/\phi^T}), \tag{15}$$

where $\Delta_\sigma = \sigma_T - \sigma$ and $\Delta_\lambda = \lambda - \lambda_c$. In turn, $\mathcal{H}$ is a scaling function and ϕ^T is the crossover critical exponent. In Fig. 6(d), we plot the rescaled order parameter $\rho\Delta_\sigma^{-\beta^T/\phi^T}$ versus $\Delta_\lambda \Delta_\sigma^{-1/\phi^T}$. We see that our MC data do collapse reasonably well which, in turn, yields the estimated values for $\beta^T = 0.49 \pm 0.01$ and $\phi^T = 0.52 \pm 0.02$.

Taking into account all the results shown in the four panels of Fig. 6 we note that the independent estimates for critical exponents are statistically consistent with each other. The best estimated values summarized in Table 2 indicate that the relations between the tricritical exponents $z^T = \nu_\parallel^T/\nu_\perp^T$, $\delta^T = \beta^T/\nu_\parallel^T$ are satisfactorily preserved. All these results show that the tricricality of the MVE on complete graphs also belongs to the TDP universality class.

4. Final remarks

We characterized the critical and tricritical phenomena associated with the dynamics of a minimal vaccination-epidemic (MVE) model. Our results obtained through a mean-field approach, MC simulations and finite-size scaling (FSS) theory revealed the presence of continuous

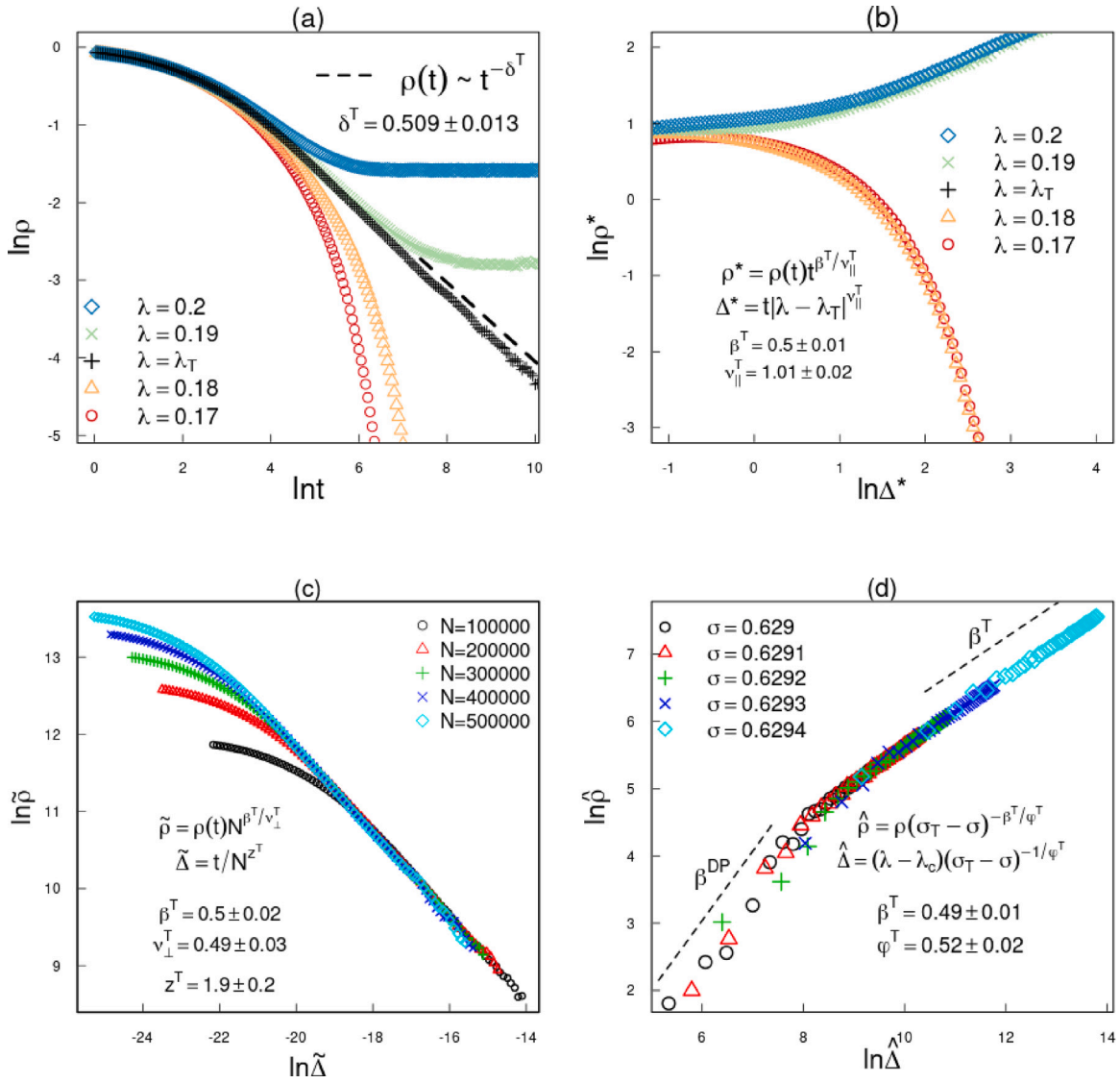

Fig. 6. Tricritical behavior for the MVE on complete graphs. To assist the FSS analysis, we use the location of the TCP obtained from Eq. (10): $\lambda_T = 0.18889$ and $\sigma_T = 0.62941$. All panels are in log–log scale. Panel (a): $\rho(t)$ versus t for simulations performed with $N = 5.10^5$ and different λ around the TCP; the black dashed line corresponds to the fit at $\lambda = \lambda_T$. Panel (b): $\rho^* = \rho(t)t^{\beta^T/\nu_{||}^T}$ versus $\Delta^* = t(\lambda - \lambda_c)^{\nu_{||}^T}$ for $N = 5.10^5$ and different λ near the TCP; the color legend of panel (a) also applies to panel (b). Panel (c): $\tilde{\rho} = \rho(t)L^{\beta^T/\nu_\perp^T}$ versus $\tilde{\Delta} = tN^{-z^T}$ for $N = \{10^5 - 5.10^5\}$ and $\lambda = \lambda_T$. Panel (d): $\hat{\rho} = \rho(\sigma_T - \sigma)^{-\beta^T/\phi^T}$ versus $\hat{\Delta} = (\lambda - \lambda_c)(\sigma_T - \sigma)^{-1/\phi^T}$ for $N = 5.10^5$; the dashed lines are guidelines to the eye with the exact slopes $\beta^{DP} = 1$ and $\beta^T = 1/2$. In all cases we use $\rho_o = 1$ and we let the simulations run until the dynamics reaches the stationary state. The estimated values for the tricritical exponents are shown inside each panel and the best values are summarized in Table 2. (For interpretation of the references to color in this figure legend, the reader is referred to the web version of this article.)

Table 1
Critical exponents of the MVE obtained from the FSS analysis presented in Fig. 5. The exponents for the Directed Percolation (DP) universality class were taken from the appendix A.3.1 of Ref. [39].

2D lattice	β	z	δ	$\nu_{\|\|}$	$\nu_\perp$
MVE	0.58 ± 0.02	1.73 ± 0.12	0.489 ± 0.082	1.29 ± 0.01	0.74 ± 0.04
DP	0.5834 ± 0.0030	1.7660 ± 0.0016	0.4505 ± 0.0010	1.295 ± 0.006	0.7333 ± 0.0075

Table 2
Tricritical exponents for the MVE obtained from the FSS analysis presented in Fig. 6. The theoretical mean-field exponents were taken from Refs. [37,38].

Complete graph	ϕ^T	β^T	δ^T	$\nu_{\|\|}^T$	$\nu_\perp^T$	z^T
Estimated	0.52 ± 0.02	0.50 ± 0.01	0.509 ± 0.013	1.01 ± 0.02	0.49 ± 0.03	1.9 ± 0.2
Expected	1/2	1/2	1/2	1	1/2	2

and discontinuous phase transitions depending on the dimensionality of the system.

Despite much theoretical progress, there is no general framework yet to treat the subject of first-order phase transitions in low-dimensional nonequilibrium systems. While this subject was clarified in 1D systems with the Hinrichsen's conjecture [40], the full picture for 2D systems is still not clear. At present it is known that, discontinuous nonequilibrium transitions into an absorbing state detected in the mean-field limit can also take place in 2D lattices [30,41–46], but this is not always the case [29,47]. For instance, recently it was shown [29] that the phase transition of the two-dimensional symbiotic contact process [48] is continuous, in disagreement with the discontinuous transition observed in the mean-field limit. Here, we show that the MVE model undergoes a first-order absorbing state transition on systems with infinite dimension, namely complete graphs and random k-regular networks. However, for the MVE model on regular square lattices, we find no signs of a discontinuous transition to the absorbing state.

Previous studies have introduced stochastic extensions of the SIS model capable of generating discontinuous transitions [47,49–57]. But none of them presented the possibility of universal features emerging at the line separating the regime of discontinuous and continuous transitions. Here, we also show that the tricritical point of the MVE on full graphs is associated with scaling laws compatible with an independent universality class, namely the Tricritical Directed Percolation (TDP) [37,38]. It is important to note that our tricritical analysis is different from the one presented in Ref. [58], where the authors studied the so-called generalized general epidemic process (GGEP) which is an extension of the SIR model with four classes of individuals. They reported that the GGEP can be tuned to fall in the universality class of the Tricritical Dynamic Isotropic Percolation (TDIP).

In summary, our work adds statistical and spatial insight into epidemic-vaccination models that present nonequilibrium continuous and discontinuous phase transitions. In future works, it would be interesting to investigate the critical phenomena arising from the MVE model in a low-dimensional system of mobile agents. As documented in previous studies [59–63], diffusion can play multiple and contrasting roles in nonequilibrium models that have active-to-absorbing phase transitions.

CRediT authorship contribution statement

Marcelo A. Pires: Conceptualization, Methodology, Investigation, Software, Data curation, Visualization, Writing – original draft. **Cesar I.N. Sampaio Filho:** Methodology, Writing – review & editing. **Hans J. Herrmann:** Conceptualization, Methodology, Writing – review & editing, Supervision. **José S. Andrade Jr.:** Conceptualization, Methodology, Writing – review & editing, Supervision.

Declaration of competing interest

The authors declare that no competing interests exist.

Data availability

All data utilized in this study was obtained through computer simulations and can be replicated using the methodology described therein.

Acknowledgments

We gratefully acknowledge CNPq, Brazil, CAPES, Brazil, FUNCAP, Brazil and the National Institute of Science and Technology for Complex Systems in Brazil for financial support.

References

[1] Wang Z, Bauch CT, Bhattacharyya S, d'Onofrio A, Manfredi P, Perc M, Perra N, Salathé M, Zhao D. Statistical physics of vaccination. Phys Rep 2016;664:1–113.
[2] Pastor-Satorras R, Castellano C, Van Mieghem P, Vespignani A. Epidemic processes in complex networks. Rev Modern Phys 2015;87(3):925.
[3] Serafino M, Monteiro HS, Luo S, Reis SD, Igual C, Lima Neto AS, Travizano M, Andrade Jr. JS, Makse HA. Digital contact tracing and network theory to stop the spread of COVID-19 using big-data on human mobility geolocalization. PLoS Comput Biol 2022;18(4):e1009865.
[4] Ponte C, Carmona HA, Oliveira EA, Caminha C, Lima AS, Andrade Jr. JS, Furtado V. Tracing contacts to evaluate the transmission of COVID-19 from highly exposed individuals in public transportation. Sci Rep 2021;11(1):1–11.
[5] S Reis SD, Böttcher L, Nogueira JPdC, Sousa GS, Lima Neto AS, Herrmann HJ, Andrade Jr. JS. Spatio-temporal characteristics of dengue outbreaks. Front Phys 2022;579.
[6] Marro J, Dickman R. Nonequilibrium Phase Transitions in Lattice Models. Cambridge University Press; 2005.
[7] Hinrichsen H. Non-equilibrium critical phenomena and phase transitions into absorbing states. Adv Phys 2000;49(7):815–958.
[8] Zhou Y, Liu H. Stability of periodic solutions for an SIS model with pulse vaccination. Math Comput Modelling 2003;38(3–4):299–308.
[9] Shaw LB, Schwartz IB. Enhanced vaccine control of epidemics in adaptive networks. Phys Rev E 2010;81:046120.
[10] Pires MA, Crokidakis N. Dynamics of epidemic spreading with vaccination: impact of social pressure and engagement. Phys A Stat Mech Appl 2017;467:167–79.
[11] Castro TTMd, Oliveira MJd. Effect of immunization through vaccination on the SIS epidemic spreading model. J Phys A 2022;55(27).
[12] Kribs-Zaleta CM, Velasco-Hernández JX. A simple vaccination model with multiple endemic states. Math Biosci 2000;164(2):183–201.
[13] Kribs-Zaleta CM, Martcheva M. Vaccination strategies and backward bifurcation in an age-since-infection structured model. Math Biosci 2002;177:317–32.
[14] Arino J, McCluskey CC, van den Driessche P. Global results for an epidemic model with vaccination that exhibits backward bifurcation. SIAM J Appl Math 2003;64(1):260–76.
[15] Brauer F. Backward bifurcations in simple vaccination models. J Math Anal Appl 2004;298(2):418–31.
[16] Sharomi O, Podder C, Gumel A, Elbasha E, Watmough J. Role of incidence function in vaccine-induced backward bifurcation in some HIV models. Math Biosci 2007;210(2):436–63.
[17] Reluga TC, Medlock J. Resistance mechanisms matter in SIR models. Math Biosci Eng 2007;4(3):553.
[18] Buonomo B, Lacitignola D. On the backward bifurcation of a vaccination model with nonlinear incidence. Nonlinear Anal Model Control 2011;16(1):30–46.
[19] Gerberry DJ. Practical aspects of backward bifurcation in a mathematical model for tuberculosis. J Theoret Biol 2016;388:15–36.
[20] Zhang Q, Tang B, Tang S. Vaccination threshold size and backward bifurcation of SIR model with state-dependent pulse control. J Theoret Biol 2018;455:75–85.
[21] Nudee K, Chinviriyasit S, Chinviriyasit W. The effect of backward bifurcation in controlling measles transmission by vaccination. Chaos Solitons Fractals 2019;123:400–12.
[22] Lacitignola D, Saccomandi G. Managing awareness can avoid hysteresis in disease spread: An application to coronavirus COVID-19. Chaos Solitons Fractals 2021;144:110739.
[23] Rashkov P, Kooi BW. Complexity of host-vector dynamics in a two-strain dengue model. J Biol Dyn 2021;15(1):35–72.
[24] Saldaña F, Velasco-Hernández JX. Modeling the COVID-19 pandemic: a primer and overview of mathematical epidemiology. SeMA J 2021;1–27.
[25] Song B. Basic reinfection number and backward bifurcation. Math Biosci Eng 2021;18(6):8064–83.
[26] Siegenfeld AF, Taleb NN, Bar-Yam Y. What models can and cannot tell us about COVID-19. Proc Natl Acad Sci 2020;117(28):16092–5.
[27] Gillespie DT. Exact stochastic simulation of coupled chemical reactions. J Phys Chem A 1977;81(25):2340–61.
[28] Macedo-Filho A, Alves G, Costa Filho R, Alves T. Reactivating dynamics for the susceptible-infected-susceptible model: a simple method to simulate the absorbing phase. J Stat Mech Theory Exp 2018;2018(4):043208.
[29] Sampaio Filho CIN, dos Santos TB, Araújo NAM, Carmona HA, Moreira AA, Andrade Jr. JS. Symbiotic contact process: Phase transitions, hysteresis cycles, and bistability. Phys Rev E 2018;98:062108.
[30] Assis VRV, Copelli M. Discontinuous nonequilibrium phase transitions in a nonlinearly pulse-coupled excitable lattice model. Phys Rev E 2009;80:061105.
[31] Janssen H-K. On the nonequilibrium phase transition in reaction-diffusion systems with an absorbing stationary state. Z. Phys B - Conden Matter 1981;42:151–4.
[32] Grassberger P. On phase transitions in Schlögl's second model. Z. Phys B - Condens Matter 1982;47:365–74.
[33] Araújo NAM, Andrade Jr. JS, Ziff RM, Herrmann HJ. Tricritical point in explosive percolation. Phys Rev Lett 2011;106:095703.

[34] Cellai D, Lawlor A, Dawson KA, Gleeson JP. Tricritical point in heterogeneous k-core percolation. Phys Rev Lett 2011;107:175703.
[35] Cao L, Schwarz JM. Correlated percolation and tricriticality. Phys Rev E 2012;86:061131.
[36] Min B, San Miguel M. Competing contagion processes: Complex contagion triggered by simple contagion. Sci Rep 2018;8(1):1–8.
[37] Lübeck S. Tricritical directed percolation. J Stat Phys 2006;123(1):193–221.
[38] Grassberger P. Tricritical directed percolation in 2+ 1 dimensions. J Stat Mech Theory Exp 2006;2006(01):P01004.
[39] Lubeck S. Universal scaling behavior of non-equilibrium phase transitions. Internat J Modern Phys B 2004;18(31n32):3977–4118.
[40] Hinrichsen H. First-order transitions in fluctuating 1+ 1-dimensional nonequilibrium systems. 2000, arXiv Preprint Cond-Mat/0006212.
[41] Windus A, Jensen HJ. Phase transitions in a lattice population model. J Phys A 2007;40(10):2287.
[42] da Silva EF, de Oliveira MJ. Critical discontinuous phase transition in the threshold contact process. J Phys A 2011;44(13):135002.
[43] da Silva EF, de Oliveira MJ. Two versions of the threshold contact model in two dimensions. Comput Phys Comm 2012;183(9):2001–5.
[44] Fiore CE. Minimal mechanism leading to discontinuous phase transitions for short-range systems with absorbing states. Phys Rev E 2014;89:022104.
[45] de Oliveira MM, da Luz MGE, Fiore CE. Generic finite size scaling for discontinuous nonequilibrium phase transitions into absorbing states. Phys Rev E 2015;92:062126.
[46] de Oliveira MM, Fiore CE. Temporal disorder does not forbid discontinuous absorbing phase transitions in low-dimensional systems. Phys Rev E 2016;94:052138.
[47] Chen L, Ghanbarnejad F, Brockmann D. Fundamental properties of cooperative contagion processes. New J Phys 2017;19(10):103041.
[48] de Oliveira MM, Dos Santos RV, Dickman R. Symbiotic two-species contact process. Phys Rev E 2012;86:011121.
[49] Böttcher L, Nagler J, Herrmann HJ. Critical behaviors in contagion dynamics. Phys Rev Lett 2017;118:088301.
[50] Dodds PS, Watts DJ. Universal behavior in a generalized model of contagion. Phys Rev Lett 2004;92:218701.
[51] Gross T, D'Lima CJD, Blasius B. Epidemic dynamics on an adaptive network. Phys Rev Lett 2006;96:208701.
[52] Böttcher L, Woolley-Meza O, Araújo NA, Herrmann HJ, Helbing D. Disease-induced resource constraints can trigger explosive epidemics. Sci Rep 2015;5(1):1–11.
[53] Chae H, Yook S-H, Kim Y. Discontinuous phase transition in a core contact process on complex networks. New J Phys 2015;17(2):023039.
[54] Gómez-Gardenes J, Lotero L, Taraskin S, Pérez-Reche F. Explosive contagion in networks. Sci Rep 2016;6(1):1–9.
[55] Chen H, Huang F, Zhang H, Li G. Epidemic extinction in a generalized susceptible-infected-susceptible model. J Stat Mech Theory Exp 2017;2017(1):013204.
[56] Pires MA, Oestereich AL, Crokidakis N. Sudden transitions in coupled opinion and epidemic dynamics with vaccination. J Stat Mech Theory Exp 2018;2018(5):053407.
[57] Matamalas JT, Gómez S, Arenas A. Abrupt phase transition of epidemic spreading in simplicial complexes. Phys Rev Res 2020;2(1):012049.
[58] Janssen H-K, Müller M, Stenull O. Generalized epidemic process and tricritical dynamic percolation. Phys Rev E 2004;70:026114.
[59] González M, Herrmann H. Scaling of the propagation of epidemics in a system of mobile agents. Phys A Stat Mech Appl 2004;340(4):741–8.
[60] Villa Martín P, Bonachela JA, Levin SA, Muñoz MA. Eluding catastrophic shifts. Proc Natl Acad Sci 2015;112(15):E1828–36.
[61] Pianegonda S, Fiore CE. Effect of diffusion in simple discontinuous absorbing transition models. J Stat Mech Theory Exp 2015;2015(8):P08018.
[62] De Oliveira M, Fiore C. Effects of diffusion in competitive contact processes on bipartite lattices. J Stat Mech Theory Exp 2017;2017(5):053211.
[63] Polovnikov B, Wilke P, Frey E. Subdiffusive activity spreading in the diffusive epidemic process. Phys Rev Lett 2022;128:078302.